

Double Dirac Nodal Line Semimetal with Torus Surface State

Xiao-Ping Li,¹ Botao Fu,² Da-Shuai Ma,¹ Chaoxi Cui,¹ Zhi-Ming Yu,^{1,*} and Yugui Yao^{1,†}

¹*Key Lab of Advanced Optoelectronic Quantum Architecture and Measurement (MOE),
Beijing Key Lab of Nanophotonics & Ultrafine Optoelectronic Systems,
and School of Physics, Beijing Institute of Technology, Beijing 100081, China*
²*College of Physics and Electronic Engineering, Center for Computational Sciences,
Sichuan Normal University, Chengdu, 610068, China*

We propose a class of nodal line semimetals that host an eight-fold degenerate double Dirac nodal line (DDNL) with negligible spin-orbit coupling. We find only 5 of the 230 space groups host the DDNL. The DDNL can be considered as a combination of two Dirac nodal lines, and has a trivial Berry phase. This leads to two possible but completely different surface states, namely, a torus surface state covering the whole surface Brillouin zone and no surface state at all. Based on first-principles calculations, we predict that the hydrogen storage material LiBH is an ideal DDNL semimetal, where the line resides at Fermi level, is relatively flat in energy, and exhibits a large linear energy range. Interestingly, both the two novel surface states of DDNL can be realized in LiBH. Further, we predict that with a magnetic field parallel to DDNL, the Landau levels of DDNL are doubly degenerate due to Kramers-like degeneracy and have a doubly degenerate zero-mode.

Introduction. The past decade has witnessed a tremendous advance in the understanding of topological band theory, for which one of the most representative and experimentally relevant realization may be topological semimetals, where novel quasi-particles, such as Weyl and Dirac fermion, appear as low-energy excitations around nontrivial crossings formed by conduction and valence bands [1–4]. Various fascinating phenomena associated with topological semimetals are predicted, such as topologically protected surface states [4, 5], unusual optical and magnetic responses [6–9], density fluctuation plasmons [10, 11], and quantized circulation of anomalous shift [12].

In three-dimensions, the band crossing, in addition to zero-dimensional (0D) nodal points [13–19], also can be 1D nodal line (NL) [20–24] or even 2D nodal surface [25–28], protected by corresponding space group (SG) symmetries. The current study of nodal line semimetals mainly focus on the case that the line is generated by band inversion, topologically protected by π Berry phase and characterized by drumhead-like surface state. Various topological nodal line semimetals belonging to this paradigm are predicted, and some of them have been experimentally confirmed [29–38]. With multiple symmetries, the nodal line can take many different forms in Brillouin zone (BZ), such as higher-order nodal line, nodal chain, crossed nodal line, nodal box and Hopf-link loop [39–51].

In this work, we theoretically propose another possibility of the nodal line, namely, double Dirac nodal line (DDNL) in 3D systems with negligible spin-orbit coupling (SOC) effect (such as the materials with atoms of carbon or even lighter than carbon). This nodal line

is four-fold degenerate (eight-fold degenerate if including spin degree of freedom) and resides at certain high-symmetry line in BZ. For each 2D plane transverse to DDNL (setting as k_x - k_y plane), the band crossing on the line can be considered as a sum of two Dirac point and its effective Hamiltonian may be written as

$$\mathcal{H} = \begin{bmatrix} h_D & h' \\ h'^{\dagger} & h_D \end{bmatrix}, \quad (1)$$

where each entry is a 2×2 submatrix and

$$h_D = v_x k_x \sigma_x + v_y k_y \sigma_y, \quad (2)$$

with σ_i ($i = x, y, z$) the Pauli matrix, and $v_x(y)$ the Fermi velocity in $x(y)$ direction. The two diagonal blocks (h_D) describe two 2D Dirac points with same topological charge (Berry phase) of π in the k_x - k_y plane, and the off-diagonal term h' denotes the coupling between the two Dirac points. While Dirac nodal line has been well studied in previous works [21, 31], the DDNL has not yet been proposed.

Generally, the electron bands in the systems without SOC effect is not degenerate. Hence, the DDNL is rather rare and requires strict symmetries for its realization. Indeed, by an exhaustive searching over 230 SGs [52], we

TABLE I. Space groups allowing for DDNL with negligible SOC effect. The DDNL is stabilized by the nonsymmorphic operators of systems. Here, $\alpha \in (0, \frac{1}{2})$

SG No.	BZ	Location
57	Γ_o	RT: $\{\alpha, \frac{1}{2}, \frac{1}{2}\}$
60	Γ_o	RU: $\{\frac{1}{2}, \alpha, \frac{1}{2}\}$
61	Γ_o	RT: $\{\alpha, \frac{1}{2}, \frac{1}{2}\}$, RU: $\{\frac{1}{2}, \alpha, \frac{1}{2}\}$, RS: $\{\frac{1}{2}, \frac{1}{2}, \alpha\}$
62	Γ_o	RS: $\{\frac{1}{2}, \frac{1}{2}, \alpha\}$
205	Γ_c	RM: $\{\frac{1}{2}, \frac{1}{2}, \alpha\}$

* zhiming_yu@bit.edu.cn

† ygyao@bit.edu.cn

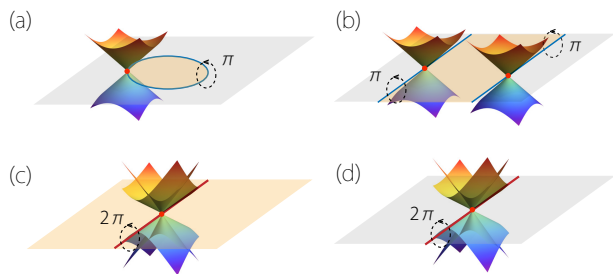


FIG. 1. Schematic showing the surface state of nodal line semimetal, as well as the electronic band around line. The orange region denotes surface state. (a) Usual Dirac NL with drumhead-like surface state. (b) A Dirac NL traversing bulk BZ should come in pair and can be considered as a variation of usual Dirac NL due to strong anisotropy. (c-d) DDNL has two possible but distinct surface states: (c) a torus surface state spanning the whole surface BZ, and (d) no surface state.

find that only 5 SGs can exhibit the DDNL, which resides along the high-symmetry line located at the boundary of BZ. The five SGs and the location of DDNL in BZ are given in Table I. Particularly, for all the five SGs, the DDNL is the only possible degeneracy at the corresponding high-symmetry line(s), indicating that the number of the electronic bands of materials belonging to these SGs must be a multiple of 8 (including spin degree of freedom). Hence, for the material belonging to these SGs and having $8n + 4$ (with n an integer) electrons, it must be a DDNL semimetal enforced by the filling [53].

The DDNL is topologically distinct from the usual Dirac nodal line (with π Berry phase) in that its Berry phase is 2π , as it can be considered as a combination of two Dirac nodal lines. Since the Berry phase is defined mod of 2π , it is trivial for DDNL. As a consequence, the DDNL features two distinct states at the boundary of system, as schematically shown in Fig. 1(c-d), which both are completely different from the drumhead-like surface state in usual NL [see Fig. 1(a-b)]. One is the novel surface state spanning over the whole surface BZ [see Fig. 1(c)]. Since the 2D surface BZ is a torus, such novel surface state then is termed as torus surface state [39, 54]. The other case is that no surface state appears on the surface, even though there exists a NL (e.g. DDNL) in bulk [see Fig. 1(d)]. These two cases are topologically allowed and consistent with the trivial Berry phase of DDNL. Moreover, we predict that by applying a magnetic field parallel to the line, the Landau levels of DDNL are doubly degenerate due to Kramers-like degeneracy and have a doubly degenerate zero-mode, which shall suggest pronounced signature in magneto-transport.

We demonstrate our ideas by the first-principles calculations and model analysis of a concrete material. We find the hydrogen storage material LiBH is an ideal DDNL semimetal candidate, where the DDNL resides at Fermi level, is relatively flat in energy, and exhibits

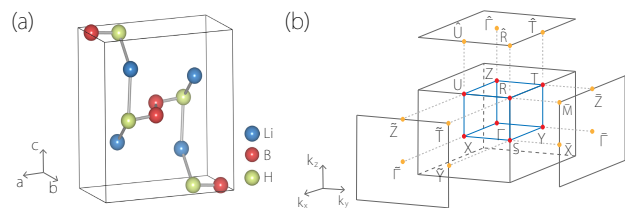


FIG. 2. (a) Crystal structure of LiBH material. (b) Bulk BZ and (100), (010) and (001) surface BZ.

a large linear energy range. Interestingly, both torus surface state and no surface state simultaneously appear in LiBH material. More importantly, we calculate the LL spectrum of a lattice model based on LiBH and find the doubly degenerate zero-mode LL can be clearly observed. These results indicate that the novel properties of DDNL predicted here should be experimentally detected in LiBH. Thus, our work not only predicts a new semimetal phase, but also shows an ideal material platform for exploring interesting fundamental physics connected to it.

Crystalline structure and electronic bands. We motivate our investigation by considering the hydrogen storage material LiBH [55]. This material has a orthorhombic structure with SG Pnma (No. 62), which is one candidate in Table I. The primitive cell of LiBH contains in total 12 atoms with Li, B and H residing at the 4c Wyck-off positions, as shown in Fig. 2(a). Since all the three atoms: Li, B and H are *lighter* than carbon, the SOC effect in LiBH is negligibly small, and we virtually obtain a spinless system. This is a precondition for realizing DDNL, as the DDNL is not robust against SOC [52]. Moreover, the electron number of LiBH is 20 ($= 2 \times 8 + 4$). Therefore, the LiBH material is a filling-enforced DDNL semimetal with the line appearing around Fermi level. The lattice constants obtained from our first-principles calculations are $a = 6.2 \text{ \AA}$, $b = 3.0 \text{ \AA}$ and $c = 6.3 \text{ \AA}$ [56], consistent with previous result [55]. The symmetry operators of SG 62 are generated by two screw rotations $C_{2z} = \{C_{2z} | \frac{1}{2}0\frac{1}{2}\}$ and $C_{2y} = \{C_{2y} | 0\frac{1}{2}0\}$, and a spatial inversion \mathcal{P} . The material also has time-reversal symmetry \mathcal{T} with $\mathcal{T}^2 = 1$, corresponding to the negligible SOC effect in LiBH.

The calculated electronic band structure of LiBH without SOC is presented in Fig. 3(a). It is clearly shown that this material is a DDNL semimetal with the line appearing at RS path, consistent with symmetry analysis (see Table I). A remarkable feature of the electronic bands of LiBH is that its low-energy spectra is roughly symmetric about Fermi level, indicating that LiBH has an approximate chiral symmetry [57]. From Fig. 3(a), one observes that there exist two band crossings almost cutting the Fermi level. We first consider the linear crossing (labelled as *A*) on ΓY path. Due to the presence of $\tilde{\mathcal{M}}_z = \tilde{C}_{2z}\mathcal{P}$ and \mathcal{PT} symmetry, point *A* can not appear

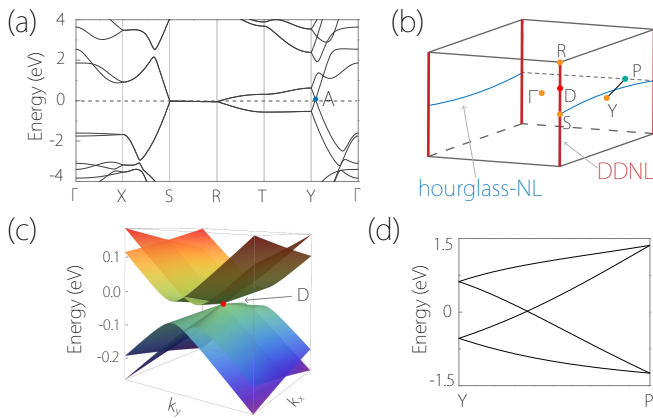


FIG. 3. (a) Electronic band structure of LiBH. (b) Schematic showing DDNL and hourglass NL. The electronic band (c) around a generic point (D) on DDNL and (d) a generic path passing through hourglass NL.

in isolation but reside on a NL in the $k_z = 0$ plane [see Fig. 3(b)]. As discussed in Ref. [58], this NL is formed by the neck crossing-point of the hourglass-like dispersion [see Fig. 3(d)] and then is termed as hourglass NL. The hourglass NL can move in the $k_z = 0$ plane but is unremovable as its two endpoints are pinned at S point.

The second and also the most striking feature of LiBH is the four-fold (eight-fold if including spin) degenerate crossing along RS path, giving rise to a DDNL at Fermi level. The DDNL is rather flat with an energy variation of 20 meV, due to the approximate chiral symmetry, and exhibits highly dispersive bands in the plane normal to the line, as shown in Fig. 3(a) and 3(c). Therefore, LiBH provides an ideal material platform to explore the novel physics associated with DDNL and hourglass NL in experiments. Although the properties of hourglass NL are similar to usual NL [41, 46], the DDNL would feature novel phenomena distinguished from usual NL, due to a trivial Berry phase and completely different low-energy spectrum. Hence, in the following we mainly focus on the investigation of the interesting properties of DDNL.

DDNL and effective Hamiltonian. Since the LiBH material exhibits three orthogonal two-fold screw rotation axes, the electronic bands at all the three boundary planes ($k_{x,y,z} = \pi$ plane) are at least doubly degenerate and the whole bulk BZ is covered by nodal surfaces [27, 59], as shown in Fig. 3(a). The DDNL sits at the hinge between $k_x = \pi$ and $k_y = \pi$ planes, e.g. the high-symmetry path RS, and then is formed by the crossing of two nodal surfaces. For a generic point (D) on RS, its symmetry operators can be generated by \tilde{C}_{2z} , $\tilde{M}_y = \{\mathcal{M}_y | 0\frac{1}{2}0\}$ and a combined operator $\mathcal{A} = \tilde{C}_{2y}\mathcal{T}$. The algebra satisfied by the three generators at D point is equivalent to that of the three generators at S point, as both D and S are interior points of RS line [52]. Then, for concise we consider the algebra of the three generators at

S point to explain the appearance of DDNL, which can be written as $\tilde{C}_{2z}^2 = \tilde{M}_y^2 = 1$, $\mathcal{A}^2 = -1$ and

$$\tilde{M}_y \tilde{C}_{2z} = -\tilde{C}_{2z} \tilde{M}_y, \tilde{C}_{2z} \mathcal{A} = \mathcal{A} \tilde{C}_{2z}, \tilde{M}_y \mathcal{A} = -\mathcal{A} \tilde{M}_y \quad (3)$$

The Bloch states at S point can be chosen as the eigenstates of \tilde{C}_{2z} , denoted as $|c_{2z}\rangle$ with $c_{2z} = \pm 1$ the eigenvalue of \tilde{C}_{2z} . Since \tilde{C}_{2z} anticommutes with \tilde{M}_y , the two states $|1\rangle$ and $|-1\rangle$ would be degenerate, as $|\pm 1\rangle = \tilde{M}_y |\mp 1\rangle$. Also as \tilde{C}_{2z} commutes with \mathcal{A} and $\mathcal{A}^2 = -1$, the state $|\pm 1\rangle$ and its Kramers-like partner $\mathcal{A}|\pm 1\rangle$ are linearly independent. Hence, the four states $\{|1\rangle, |-1\rangle, \mathcal{A}|1\rangle, \mathcal{A}|-1\rangle\}$ must be degenerate at the same energy, forming a DDNL along RS path. Based on the quartet basis, the matrix representations of the generators can be expressed as

$$\tilde{C}_{2z} = \sigma_0 \otimes \sigma_z, \tilde{M}_y = \sigma_z \otimes \sigma_x, \mathcal{A} = i\sigma_y \otimes \sigma_0 \mathcal{K}, \quad (4)$$

with \mathcal{K} the complex conjugation. With the standard approach [19, 60], the effective $k \cdot p$ Hamiltonian for a generic point on DDNL can be obtained as

$$\mathcal{H}_{\text{DDNL}} = (c_1 + c_2 k_z) + \begin{bmatrix} h_D & h' \\ h'^\dagger & h_D \end{bmatrix}, \quad (5)$$

with $h_D = c_3 k_x \sigma_x + c_4 k_y \sigma_y$ and $h' = \alpha k_x \sigma_y + \beta k_y \sigma_x$. Here, $c_{i=1,2,3,4}$ is real parameter, and α and β are complex parameters. Clearly, the obtained Hamiltonian (5) is consistent with Eq. (1) in Introduction, which directly demonstrates the existence of DDNL in LiBH. Due to nonvanishing off-diagonal term h' , the two Dirac cones described by h_D would split at a general momentum point, while are stucked together along $k_{x(y)} = 0$ axis [see Fig. 3(c)], resulting from the nodal surfaces on boundaries.

Torus surface state. We then explore the surface state of LiBH. It has been extensively shown that NL semimetals feature drumhead-like surface state at sample boundary, due to π Berry phase of the line. This is the case for the hourglass NL in LiBH, which has π Berry phase and leads a drumhead-like surface state at (001) surface, as shown in Fig. 4(c,f). However, both (100) and (010) surfaces, which are parallel to DDNL, do not exhibit drumhead-like surface state. More surprisingly, the (100) surface has a torus surface state covering the whole (100) surface BZ, as shown in Fig. 4(a,d), and in sharp contrast, the (010) surface does not have any surface state [Fig. 4(b,e)].

The surface state in NL semimetal generally is protected by quantized π Zak phase, which is the Berry phase of a straight line normal to the surface and crossing the bulk BZ [61]. Here, due to the presence of \mathcal{P} symmetry in LiBH, the Zak phase is quantized to be 0 or π , corresponding two topologically distinct phases.

We first study the surface state on (100) surface. Starting from the Zak phase $\mathcal{Z}(k_y = 0, k_z)$ (with $k_z \neq 0$) of

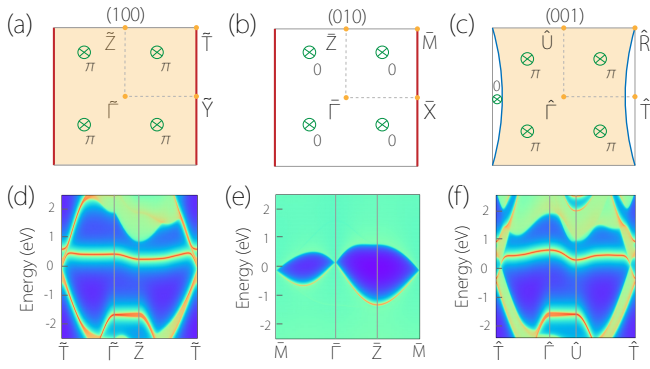


FIG. 4. (a-c) Schematic figures of the surface state for (100), (010) and (001) surfaces. The values 0 and $\pm\pi$ in (a-c) are the Zak phase for lines normal to the corresponding surface. (d-f) Surface spectra on (100), (010) and (001) surfaces. In (d), the surface state spans the whole surface BZ, leading to the torus surface state, while in (e) no surface state can be observed.

a straight line transverse to (100) surface, which is obtained as π in LiBH material [see Fig. 4(a)]. By moving the straight line along k_y -axis, the Zak phase shall not change its value until the line passes through DDNL at RS path ($k_y = \pi$). The changed value equals to the Berry phase of DDNL, namely, 2π . This means that one always has $\mathcal{Z}(k_y > \pi, k_z) = \mathcal{Z}(k_y < \pi, k_z)$, as the Zak phase is defined mod 2π . Similarly, by moving the straight line along k_z -axis, the Zak phase would change its value by zero when the line crosses over the hourglass NL at $k_z = 0$ plane. Therefore, the Zak phase $\mathcal{Z}(k_y, k_z) = \pi$ for any gapped state, resulting in a torus surface state in (100) surface, as shown in Fig. 4(a,d). Similar analysis applies for (010) surface, except that $\mathcal{Z}(k_x, k_z) = 0$ for each gapped state. Hence, no surface state can be found on this surface, as shown in Fig. 4(b,e). These unusual surface properties also can be inferred from the geometry structure of DDNL. Unlike the usual NL shown in Fig. 1(a-b) and Fig. 4(c), the projection of DDNL can not separate the corresponding surface BZ as two parts [see Fig. 4(a,b)], as the BZ is periodic. Hence, for the surface parallel to DDNL, the whole surface BZ would share same topological properties, leading to a torus surface state or no surface state on the boundary of system.

Landau spectrum. The topological feature of NL also can reflect in its magnetotransport [62, 63]. By applying a magnetic field parallel to DDNL, the electronic bands are quantized into discrete Landau levels (LLs). Generally, one can investigate the LLs of DDNL in a k_z -fixed plane, where the low-energy Hamiltonian is captured by Eq. (5). It is well known that the Dirac Hamiltonian h_D features a zero-mode LL [64]. One may wonder that the zero-mode LL would not appear in DDNL, due to the presence of the coupling h' between the two Dirac equation. However, this is not the case. We find that the

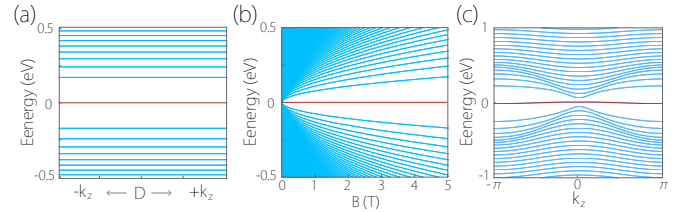


FIG. 5. (a-b) Landau spectrum with (a) different k_z ($B = 5$ T) and (b) different B (at $k_z = 0$ plane) based on the effective model (5). (c) Landau spectrum of a lattice model based on LiBH with $B = 0.01 \frac{\phi_0}{a \times b}$ (ϕ_0 is magnetic flux quantum h/e). The red curves denote doubly degenerate zero-mode LLs. The calculation details are presented in [56].

DDNL also has a zero-mode LL for each k_z -fixed plane [56], as shown in Fig. 5(a,b). Moreover, these zero-mode LLs are doubly degenerate. While the B field breaks both \mathcal{T} and $\tilde{\mathcal{C}}_{2y}$ symmetries, it preserves \mathcal{A} ($= \tilde{\mathcal{C}}_{2y}\mathcal{T}$) symmetry, and then all the LL bands (including zero-mode LLs) of DDNL are doubly degenerate resulting from the Kramers-like degeneracy produced by $\mathcal{A}^2 = -1$. Since the degeneracy of the two zero-mode LLs is protected by \mathcal{A} symmetry, it would be robust against B field and always exist regardless of the field strength. Given the fact that the zero-mode LL in graphene gives rise to many novel phenomena [64], one can expect the DDNL may exhibit interesting magnetoresponses distinct from the usual Dirac NLs and also 2D Dirac semimetal.

Particularly, the low-energy spectrum of LiBH is so clean that the LL properties proposed here shall be observed in it. We further demonstrate it by calculating the LL spectrum of a lattice model based on LiBH material. The calculated results are given in Fig. 5(c), where a doubly degenerate LL with almost flat dispersion occurring at the Fermi level, corresponding to the doubly degenerate zero-mode LL. This strongly suggests that the unusual LL spectrum of DDNL can be detected in LiBH by magnetotransport measurements.

Conclusion. In summary, we propose a new class of semimetal phase: DDNL in LiBH material. The DDNL can be considered as a combination of two Dirac NLs and exhibits many distinct phenomena, such as torus surface state and unusual LL spectrum. In particular, we predict LiBH material is an ideal DDNL semimetal and demonstrate that the novel phenomena of DDNL predicted here can be clearly observed in LiBH material. Moreover, as the torus surface in LiBH is rather flat in energy [see Fig. 4(a)], it will be interesting to explore possible unconventional superconductivity, correlation effect and magnetism in LiBH (100) surface.

The authors thank J. Xun for helpful discussions. This work is supported by the National Key R&D Program of China (Grant Nos. 2020YFA0308800, 2016YFA0300600), the NSF of China (Grants Nos. 12061131002, 11734003), the Strategic Priority Research

Program of Chinese Academy of Sciences (Grant No. XDB30000000) and Beijing Institute of Technology Research Fund Program for Young Scholars.

-
- [1] C.-K. Chiu, J. C. Y. Teo, A. P. Schnyder, and S. Ryu, Classification of topological quantum matter with symmetries, *Reviews of Modern Physics* **88**, 035005 (2016).
- [2] A. Burkov, Topological semimetals, *Nature materials* **15**, 1145 (2016).
- [3] A. Bernevig, H. Weng, Z. Fang, and X. Dai, Recent progress in the study of topological semimetals, *Journal of the Physical Society of Japan* **87**, 041001 (2018).
- [4] N. P. Armitage, E. J. Mele, and A. Vishwanath, Weyl and dirac semimetals in three-dimensional solids, *Rev. Mod. Phys.* **90**, 015001 (2018).
- [5] X. Wan, A. M. Turner, A. Vishwanath, and S. Y. Savrasov, Topological semimetal and fermi-arc surface states in the electronic structure of pyrochlore iridates, *Phys. Rev. B* **83**, 205101 (2011).
- [6] A. Burkov, Chiral anomaly and transport in weyl metals, *Journal of Physics: Condensed Matter* **27**, 113201 (2015).
- [7] F. de Juan, A. G. Grushin, T. Morimoto, and J. E. Moore, Quantized circular photogalvanic effect in weyl semimetals, *Nature communications* **8**, 1 (2017).
- [8] Z.-M. Yu, Y. Yao, and S. A. Yang, Predicted unusual magnetoresponse in type-ii weyl semimetals, *Physical review letters* **117**, 077202 (2016).
- [9] N. Nagaosa, T. Morimoto, and Y. Tokura, Transport, magnetic and optical properties of weyl materials, *Nature Reviews Materials* **5**, 621 (2020).
- [10] E. H. Hwang and S. Das Sarma, Dielectric function, screening, and plasmons in two-dimensional graphene, *Phys. Rev. B* **75**, 205418 (2007).
- [11] J. Zhou, H.-R. Chang, and D. Xiao, Plasmon mode as a detection of the chiral anomaly in weyl semimetals, *Phys. Rev. B* **91**, 035114 (2015).
- [12] Y. Liu, Z.-M. Yu, C. Xiao, and S. A. Yang, Quantized circulation of anomalous shift in interface reflection, *Phys. Rev. Lett.* **125**, 076801 (2020).
- [13] S. Murakami, Phase transition between the quantum spin hall and insulator phases in 3d: emergence of a topological gapless phase, *New Journal of Physics* **9**, 356 (2007).
- [14] S. M. Young, S. Zaheer, J. C. Y. Teo, C. L. Kane, E. J. Mele, and A. M. Rappe, Dirac semimetal in three dimensions, *Physical review letters* **108**, 140405 (2012).
- [15] Z. Wang, Y. Sun, X.-Q. Chen, C. Franchini, G. Xu, H. Weng, X. Dai, and Z. Fang, Dirac semimetal and topological phase transitions in a 3 bi ($a=na, k, rb$), *Physical Review B* **85**, 195320 (2012).
- [16] Z. Wang, H. Weng, Q. Wu, X. Dai, and Z. Fang, Three-dimensional dirac semimetal and quantum transport in $cd\ 3$ as 2 , *Physical Review B* **88**, 125427 (2013).
- [17] H. Weng, C. Fang, Z. Fang, B. A. Bernevig, and X. Dai, Weyl semimetal phase in noncentrosymmetric transition-metal monophosphides, *Physical Review X* **5**, 011029 (2015).
- [18] W. Meng, X. Zhang, T. He, L. Jin, X. Dai, Y. Liu, and G. Liu, Ternary compound $hfcup$: An excellent weyl semimetal with the coexistence of type-i and type-ii weyl nodes, *Journal of Advanced Research* (2020).
- [19] B. Bradlyn, J. Cano, Z. Wang, M. Vergniory, C. Felser, R. J. Cava, and B. A. Bernevig, Beyond dirac and weyl fermions: Unconventional quasiparticles in conventional crystals, *Science* **353** (2016).
- [20] A. A. Burkov, M. D. Hook, and L. Balents, Topological nodal semimetals, *Physical Review B* **84**, 235126 (2011).
- [21] Y. Kim, B. J. Wieder, C. L. Kane, and A. M. Rappe, Dirac line nodes in inversion-symmetric crystals, *Physical review letters* **115**, 036806 (2015).
- [22] H. Weng, Y. Liang, Q. Xu, R. Yu, Z. Fang, X. Dai, and Y. Kawazoe, Topological node-line semimetal in three-dimensional graphene networks, *Physical Review B* **92**, 045108 (2015).
- [23] C. Fang, H. Weng, X. Dai, and Z. Fang, Topological nodal line semimetals, *Chinese Physics B* **25**, 117106 (2016).
- [24] R. Li, H. Ma, X. Cheng, S. Wang, D. Li, Z. Zhang, Y. Li, and X.-Q. Chen, Dirac node lines in pure alkali earth metals, *Phys. Rev. Lett.* **117**, 096401 (2016).
- [25] Q.-F. Liang, J. Zhou, R. Yu, Z. Wang, and H. Weng, Node-surface and node-line fermions from nonsymmorphic lattice symmetries, *Physical Review B* **93**, 085427 (2016).
- [26] C. Zhong, Y. Chen, Y. Xie, S. A. Yang, M. L. Cohen, and S. Zhang, Towards three-dimensional weyl-surface semimetals in graphene networks, *Nanoscale* **8**, 7232 (2016).
- [27] W. Wu, Y. Liu, S. Li, C. Zhong, Z.-M. Yu, X.-L. Sheng, Y. X. Zhao, and S. A. Yang, Nodal surface semimetals: Theory and material realization, *Physical Review B* **97**, 115125 (2018).
- [28] X. Zhang, Z.-M. Yu, Z. Zhu, W. Wu, S.-S. Wang, X.-L. Sheng, and S. A. Yang, Nodal loop and nodal surface states in the $ti\ 3$ al family of materials, *Physical Review B* **97**, 235150 (2018).
- [29] M. Ezawa, Loop-nodal and point-nodal semimetals in three-dimensional honeycomb lattices, *Phys. Rev. Lett.* **116**, 127202 (2016).
- [30] H. Huang, J. Liu, D. Vanderbilt, and W. Duan, Topological nodal-line semimetals in alkaline-earth stannides, germanides, and silicides, *Phys. Rev. B* **93**, 201114(R) (2016).
- [31] L. M. Schoop, M. N. Ali, C. Straßer, A. Topp, A. Varykhalov, D. Marchenko, V. Duppel, S. S. P. Parkin, B. V. Lotsch, and C. R. Ast, Dirac cone protected by non-symmorphic symmetry and three-dimensional dirac line node in $zrsis$, *Nat. Commun.* **7**, 11696 (2016).
- [32] G. Bian, T.-R. Chang, R. Sankar, S.-Y. Xu, H. Zheng, T. Neupert, C.-K. Chiu, S.-M. Huang, G. Chang, I. Belopolski, *et al.*, Topological nodal-line fermions in spin-orbit metal $pbtase\ 2$, *Nature communications* **7**, 1 (2016).
- [33] S. Li, Z.-M. Yu, Y. Liu, S. Guan, S.-S. Wang, X. Zhang, Y. Yao, and S. A. Yang, Type-ii nodal loops: Theory and material realization, *Phys. Rev. B* **96**, 081106(R) (2017).
- [34] Q. Xu, R. Yu, Z. Fang, X. Dai, and H. Weng, Topological nodal line semimetals in the $cap\ 3$ family of materials, *Physical Review B* **95**, 045136 (2017).
- [35] D.-S. Ma, J. Zhou, B. Fu, Z.-M. Yu, C.-C. Liu, and Y. Yao, Mirror protected multiple nodal line semimetals and material realization, *Physical Review B* **98**, 201104(R) (2018).
- [36] T. He, X. Zhang, Y. Liu, X. Dai, G. Liu, Z.-M. Yu, and Y. Yao, Ferromagnetic hybrid nodal loop and switchable type-i and type-ii weyl fermions in two dimensions, *Physical Review B* **102**, 075133 (2020).

- [37] R.-W. Zhang, Z. Zhang, C.-C. Liu, and Y. Yao, Nodal line spin-gapless semimetals and high-quality candidate materials, *Phys. Rev. Lett.* **124**, 016402 (2020).
- [38] L. Jin, X. Zhang, Y. Liu, X. Dai, L. Wang, and G. Liu, Fully spin-polarized double-weyl fermions with type-iii dispersion in the quasi-one-dimensional materials $x_2\text{Rh}_6$ ($x = \text{k, rb, cs}$), *Physical Review B* **102**, 195104 (2020).
- [39] Z.-M. Yu, W. Wu, X.-L. Sheng, Y. X. Zhao, and S. A. Yang, Quadratic and cubic nodal lines stabilized by crystalline symmetry, *Phys. Rev. B* **99**, 121106(R) (2019).
- [40] T. Bzdušek, Q. Wu, A. Rüegg, M. Sigrist, and A. A. Soluyanov, Nodal-chain metals, *Nature* **538**, 75 (2016).
- [41] S.-S. Wang, Y. Liu, Z.-M. Yu, X.-L. Sheng, and S. A. Yang, Hourglass dirac chain metal in rhenium dioxide, *Nature communications* **8**, 1 (2017).
- [42] R. Yu, Q. Wu, Z. Fang, and H. Weng, From nodal chain semimetal to weyl semimetal in hfc , *Physical review letters* **119**, 036401 (2017).
- [43] R. Yu, H. Weng, Z. Fang, X. Dai, and X. Hu, Topological node-line semimetal and dirac semimetal state in antiperovskite Cu_3PdN , *Physical review letters* **115**, 036807 (2015).
- [44] S. Kobayashi, Y. Yamakawa, A. Yamakage, T. Inohara, Y. Okamoto, and Y. Tanaka, Crossing-line-node semimetals: General theory and application to rare-earth trihydrides, *Phys. Rev. B* **95**, 245208 (2017).
- [45] X.-L. Sheng, Z.-M. Yu, R. Yu, H. Weng, and S. A. Yang, d orbital topological insulator and semimetal in the antiferromagnetic Cu_2S family: Contrasting spin helicities, nodal box, and hybrid surface states, *The journal of physical chemistry letters* **8**, 3506 (2017).
- [46] B. Fu, X. Fan, D. Ma, C.-C. Liu, and Y. Yao, Hourglasslike nodal net semimetal in Ag_2BiO_3 , *Physical Review B* **98**, 075146 (2018).
- [47] W. Chen, H.-Z. Lu, and J.-M. Hou, Topological semimetals with a double-helix nodal link, *Physical Review B* **96**, 041102(R) (2017).
- [48] Z. Yan, R. Bi, H. Shen, L. Lu, S.-C. Zhang, and Z. Wang, Nodal-link semimetals, *Physical Review B* **96**, 041103(R) (2017).
- [49] G. Chang, S.-Y. Xu, X. Zhou, S.-M. Huang, B. Singh, B. Wang, I. Belopolski, J. Yin, S. Zhang, A. Bansil, *et al.*, Topological hopf and chain link semimetal states and their application to Co_2MnGa , *Physical review letters* **119**, 156401 (2017).
- [50] P.-Y. Chang and C.-H. Yee, Weyl-link semimetals, *Physical Review B* **96**, 081114(R) (2017).
- [51] Z. Yan, R. Bi, H. Shen, L. Lu, S.-C. Zhang, and Z. Wang, Nodal-link semimetals, *Phys. Rev. B* **96**, 041103(R) (2017).
- [52] C. Bradley and A. Cracknell, *The mathematical theory of symmetry in solids: representation theory for point groups and space groups* (Oxford University Press, 2009).
- [53] H. Watanabe, H. C. Po, M. P. Zaletel, and A. Vishwanath, Filling-enforced gaplessness in band structures of the 230 space groups, *Physical review letters* **117**, 096404 (2016).
- [54] S. S. Wang, W. K. Wu, and S. Y. Yang, Progress on topological nodal line and nodal surface, *Acta Physica Sinica* **68** (2019).
- [55] J. K. Kang, S. Y. Kim, Y. S. Han, R. P. Muller, and W. A. Goddard III, A candidate LiBH_4 for hydrogen storage: Crystal structures and reaction mechanisms of intermediate phases, *Applied Physics Letters* **87**, 111904 (2005).
- [56] See Supplemental Material for the computational methods, the tight-binding model, and the Landau levels.
- [57] X.-L. Sheng, C. Chen, H. Liu, Z. Chen, Z.-M. Yu, Y. X. Zhao, and S. A. Yang, Two-dimensional second-order topological insulator in graphdiyne, *Physical Review Letters* **123**, 256402 (2019).
- [58] R. Takahashi, M. Hirayama, and S. Murakami, Spinless hourglass nodal-line semimetals, *Physical Review B* **96**, 155206 (2017).
- [59] Z.-M. Yu, W. Wu, Y. X. Zhao, and S. A. Yang, Circumventing the no-go theorem: A single weyl point without surface fermi arcs, *Physical Review B* **100**, 041118(R) (2019).
- [60] W. Wu, Z.-M. Yu, X. Zhou, Y. X. Zhao, and S. A. Yang, Higher-order dirac fermions in three dimensions, *Physical Review B* **101**, 205134 (2020).
- [61] Y.-H. Chan, C.-K. Chiu, M. Y. Chou, and A. P. Schnyder, Ca_3P_2 and other topological semimetals with line nodes and drumhead surface states, *Physical Review B* **93**, 205132 (2016).
- [62] H. Yang, R. Moessner, and L.-K. Lim, Quantum oscillations in nodal line systems, *Physical Review B* **97**, 165118 (2018).
- [63] X. Zhang, Z.-M. Yu, Y. Lu, X.-L. Sheng, H. Y. Yang, and S. A. Yang, Hybrid nodal loop metal: Unconventional magnetoresistance and material realization, *Physical Review B* **97**, 125143 (2018).
- [64] M. O. Goerbig, Electronic properties of graphene in a strong magnetic field, *Reviews of Modern Physics* **83**, 1193 (2011).